The initiation of strain localisation in plagioclase-rich rocks: Insights from detailed microstructural analyses

H. Svahnberg*, S. Piazolo

Department of Geological Sciences, Stockholm University, SE-106 91 Stockholm, Sweden

ARTICLE INFO

ABSTRACT

In order to shed light on the cause for onset of strain localisation in plagioclase-rich rocks we have performed detailed microstructural analyses on a sheared anorthosite–leucogabbro using optical microscopy, electron backscatter diffraction (EBSD) and chemical analyses. The analysed sample is from an Archaean unit, SW Greenland, deformed at lower to mid crustal conditions ($T = 675–700\ ^\circ$C and moderate pressure). The initial deformation occurred dominantly by dislocation creep and the grain size was reduced primarily by subgrain rotation recrystallisation. Recrystallised plagioclase grains (average size 80 μm) are dominantly found in (i) clusters, (ii) lenses and (iii) continuous bands subparallel to shear zone boundaries. Recrystallised grains in clusters and lenses display inherited crystallographic orientations. Their bulk crystallographic preferred orientation (CPO) is random; however, crystallographic characteristics show that parent and daughter grains have the same misorientation axes and possibly the same active slip systems. Recrystallised grains in continuous bands show a CPO with a single dominant active slip system, (001)<110>, aligned with the structural (XYZ) framework. For these parent and daughter grains, misorientation axes are random and the dominant slip system is different. Grain rotations of recrystallised grains are traceable back to the orientation of the adjacent porphyroclast.

We infer that the cause for strain localisation is recrystallisation and development of a CPO in continuous recrystallised bands. Microstructures in combination with misorientation and slip system analyses indicate a possible change from dislocation creep in clusters and lenses to dislocation-accommodated grain boundary sliding (DisGBS) in continuous bands. This inferred shift in dominant deformation mechanism would lower the strength of the shear zone.

© 2010 Elsevier Ltd. All rights reserved.

1. Introduction

Feldspars are the most abundant minerals in the crust and are therefore important minerals when deciphering crustal rheologies (Tullis, 2002). Plagioclase feldspars are common in the lower crust and several studies of plagioclase have been undertaken to evaluate its behaviour during deformation and role in strain partitioning (e.g. Tullis and Yund, 1985; Ji and Mainpraice, 1988; Heidelbach et al., 2000; Kruse et al., 2001; Rybacki and Dresen, 2004; Baratoux et al., 2005; Mehl and Hirth, 2008; Kanagawa et al., 2008). Nevertheless, the control of slip system activation is still poorly constrained although several studies have identified important slip systems (e.g. Marshall and McLaren, 1977; Montardi and Mainprice, 1987; Stünitz et al., 2003).

Strain localisation predominantly occurs in faults and shear zones (e.g. White et al., 1980) and represents a mechanical weakening of the rock. One of the main factors contributing to strain localisation is grain size reduction (Rutter and Brodie, 1988; Montési and Hirth, 2003). The importance of grain size reduction lies in the possible change in deformation mechanism, from grain size insensitive dislocation creep to grain size sensitive diffusion creep (with grain boundary sliding, GBS), that lowers the strength of a shear zone (e.g. De Bresser et al., 2001; Kenkmann and Dresen, 2002; Raimbourg et al., 2008).

Unequivocal microstructural criteria for determination of the dominant deformation mechanism do not exist since several mechanisms may operate simultaneously (e.g. Warren and Hirth, 2006; Dimanov et al., 2007). However, some microstructures are indicative of the involvement of certain mechanisms, e.g. lattice distortions and subgrain boundaries for dislocation creep and phase mixing for GBS (e.g. Kenkmann and Dresen, 2002; Dimanov et al., 2007; and references therein). Rocks subjected to recrystallisation during intracrystalline plastic deformation display a crystallographic preferred orientation (CPO) that can be used to infer the operative deformation mechanism and the active/dominant

* Corresponding author. Tel.: +46 8 674 78 48; fax: +46 8 674 78 97.
  E-mail address: henrik.solgevik@geo.su.se (H. Svahnberg).

slip systems (e.g. Passchier and Trouw, 2005). However, recent experimental studies of anorthite aggregates have shown that a CPO may also develop with a stress exponent of $n = 1$, resembling Newtonian creep (Gómez Barreiro et al., 2007). The electron backscatter diffraction system (EBSD) has proven successful to aid microstructural interpretations by supplying information on grain orientation relationships, since most processes have specific crystallographic relationships (e.g. Wheeler et al., 2001; Bestmann and Prior, 2003). In addition, analyses of crystal lattice misorientations across subgrain boundaries can help to determine the dominant slip system (Prior et al., 2002).

The aim of this contribution is to investigate the operative deformation mechanisms and slip systems in plagioclase porphyroclasts and recrystallised grains to understand the process of recrystallisation and the development of strain localisation in a plagioclase-rich rock. We use CPO and misorientation data collected automatically by the EBSD technique in combination with microstructural characterisation and chemical analyses.

2. Geological setting and sample description

The sample for this study was collected from an amphibole-bearing anorthosite-leucogabbro unit at Qarliit Nunaat in southern West Greenland (Fig. 1a–c). The area is part of the North Atlantic craton of Archaean rocks and a current terrane model proposed for the region (e.g. Friend et al., 1987; Friend and Nutman, 2005) locates the sample site in the Tasiusarsuaq terrane (age 2920–2810 Ma; Nutman et al., 1989).

The area is structurally dominated by regional-scale tight to isoclinal upright folds and the sample site is located on a sub-vertical fold limb structurally below inferred supracrustal units and structurally above the tonalitic orthogneiss (Fig. 1c; Lee et al., 2006). At least two major phases of ductile deformation have affected the area (D1 + D2) and possibly two high grade metamorphic events, an earlier upper amphibolite to granulite facies event (M1) and a peak granulite facies metamorphism at about 2810–2790 Ma (M2; e.g Crowley, 2002). The tonalite dominating the area has orthopyroxene in the matrix and in felsic veins, indicating crystallisation at high temperature metamorphic conditions. It is interpreted to be emplaced syn-/late tectonic during the peak metamorphic event (D2 + M2) and possibly concurrently with the regional folding. The area is at present mostly at upper amphibolite to granulite facies but with some local retrogression to amphibolite and greenschist facies metamorphism (D3 + M3). Combined field relationships and structures suggest a transpressional regime. PT estimates calculated from bt–grt–sil bearing metapelite at the

north-western tip of the anorthosite-leucogabbro yielded a temperature of 675–700 °C and pressure of 350–450 MPa (Jaconelli, 2009).

The sampled anorthositic unit is more than 300 m wide and dominated by an anastamosing shear zone network of centimeter to meter sized higher strain areas surrounding less deformed lenses (Fig. 2a). These anastamosing shear zones are continuous along the deformed unit. Mylonitic foliation is sub-vertical, striking NW-SE and subparallel to shear zone boundaries, and defined by alternating compositional bands of plagioclase and aggregates of amphiboles and quartz ribbons in the central parts of the high strain zone. These quartz ribbons (up to 4 mm wide) are interpreted to be associated with the orthopyroxene-bearing tonalite intrusion and to have been emplaced as veins late during D2. Lineation defined by alignment of amphiboles is weak and trends to the SE. Our hand sample (hso468022) consists of a 10 cm thick fine-grained high strain zone between less deformed regions of leucogabbro-anorthosite. The less deformed parts contain centimeter-sized magmatic plagioclase crystals with recrystallised rims of relatively large grains (>600 μm; Fig. 2b). Mafic minerals define a bending of an older foliation into the shear zone where there is a further grain size reduction of plagioclase and development of the mylonitic foliation (Fig. 2b).

We selected two representative thin sections, hso468022D and hso468022L, for a detailed study of the microstructural development using the EBSD technique (Fig. 2b). These sections show a progressive increase in the number of recrystallised grains that are present as small clusters, lenses and as mylonitic foliation-defining continuous bands. This sequence is interpreted to represent initial development of strain localisation. Because quartz veins were emplaced later during deformation, the strain localisation was shifted from the continuous bands to the weaker quartz ribbons. Later reactivation of the shear zones (D3 + M3) continued to localise the strain, at least partly, in the quartz ribbons, preserving the high temperature deformation microstructures in the anorthosite-leucogabbro. Thin sections were cut perpendicular to the mylonitic foliation and the large-scale shear zone boundaries and parallel to the inferred shear direction, i.e. structural XYZ framework (Fig. 2b).

3. Methods

3.1. Optical microscopy

Optical microscopy was used to characterise microstructures and to distinguish areas representing the high temperature events
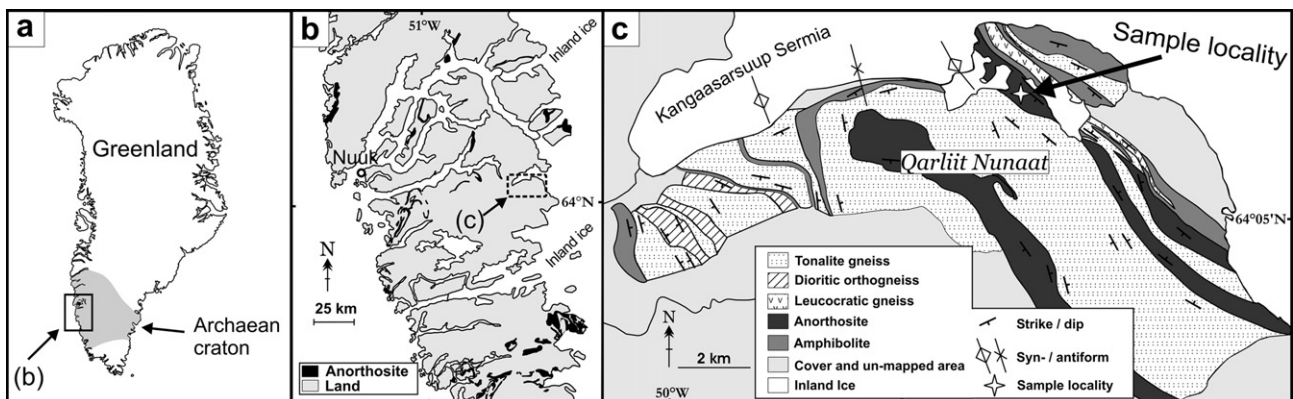

Fig. 1. Field and sample locality in the Archaean craton of Southern west Greenland. **a)** Map of Greenland, **b)** Close up of Southern West Greenland (modified after Owens and Dymek, 1997) **c)** Local geology at Qarliit Nunaat (simplified after Lee et al., 2006) and sample locality.
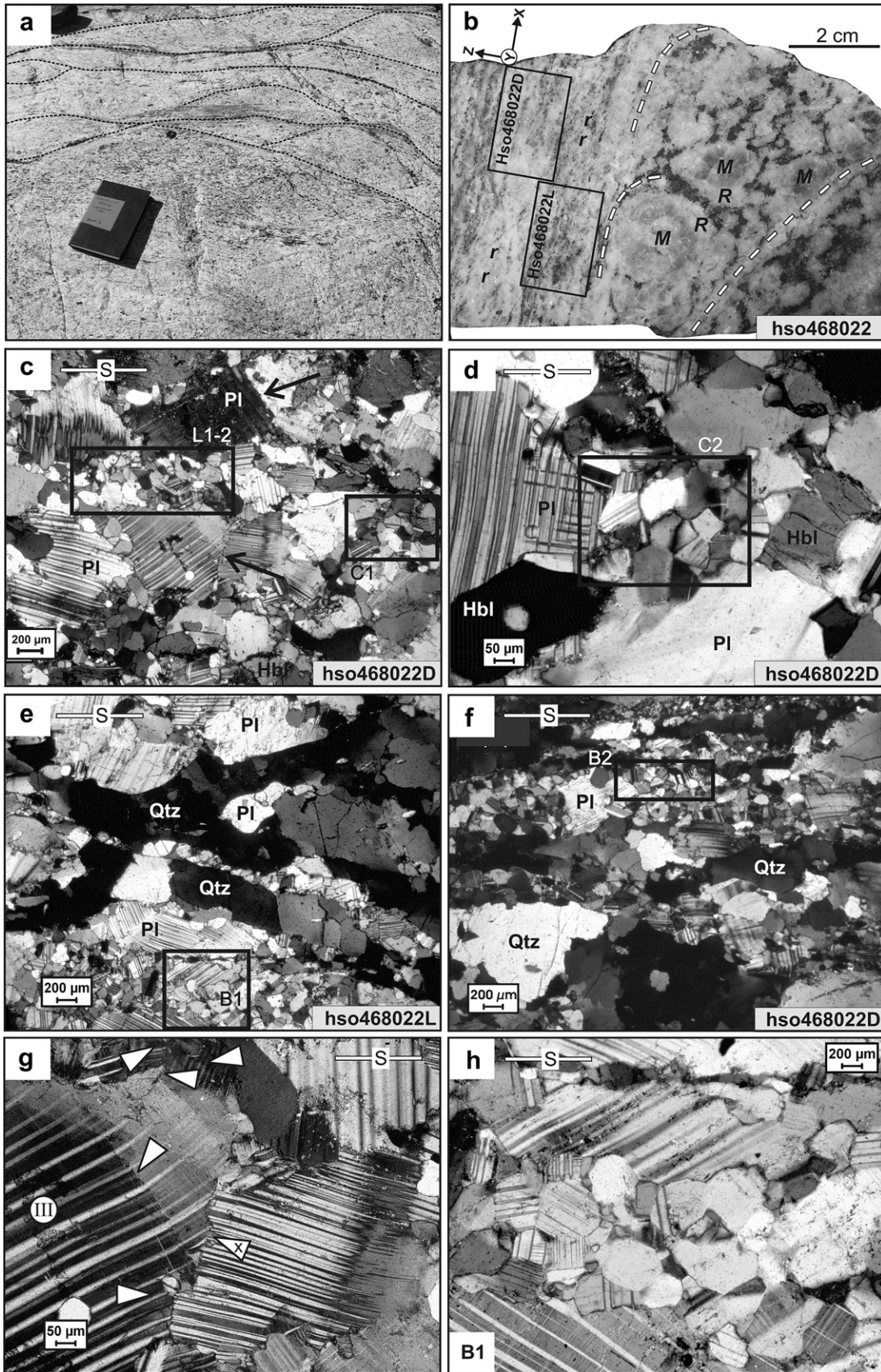
Fig. 2. **a)** Photo of the sample locality showing anastamosing network (stippled lines) of cm's-dm's high strain zones around less deformed parts of anorthosite-leucogabbro. Book (17 cm) for scale. **b)** Hand specimen hso468022. Magmatic grains (M) with brighter recrystallised (R) rims in less deformed parts and foliated finer grained part of completely recrystallised (r) plagioclase and mafic minerals. Black boxes are positions of thin sections studied. Stippled white lines show drag into shear zone. Note structural reference frame

(D2 + M2) from those affected by later lower grade overprinting (D3 + M3). Mineral abbreviations follow Kretz (1983).

3.2. Mineral chemistry

Chemical compositions of feldspars were analysed using a JEOL Superprobe JXL 8200 at University of Copenhagen. Standard online ZAF-correction was performed during acquisition and the analytical conditions used were a 15 kV acceleration voltage, 10 nA sample current and 10s counting time for peak and background using a 5 μm beam spot size.

3.3. Electron backscatter diffraction (EBSD) analyses

Crystallographic data were collected using the SEM-based EBSD technique (Adams et al., 1993; Prior et al., 1999). Analyses were performed on uncoated thin sections at Stockholm University using a Phillips XL-30 FEG-ESEM equipped with a Nordlys detector and Channel 5 analysis suite from HKL Technology (Oxford instruments). Thin-sections were chemically polished using colloidal silica before analyses. SEM-EBSD settings used were a working distance of 20–22 mm and an accelerating voltage of 20 keV corresponding to ~0.8 nA. For Pl, triclinic Andesine (Fitz Gerald et al., 1986) was used as a match unit and compared against 70 theoretical reflectors. A step size of 2 μm (if not otherwise stated) was used during automated data collections in a rectangular grid using a beam scan.

Six EBSD maps (Fig. 2c–f) were collected over assemblages of recrystallised grains and neighbouring Pl porphyroclasts. To increase the statistics, 140 additional EBSD maps with a step size of 10–20 μm were collected.

3.3.1. Processing and presentation of EBSD data

The raw EBSD data acquired automatically were processed to remove false data and to enhance the continuity of data over the microstructures. Processing followed the procedure described in Prior et al. (2002) and Bestmann and Prior (2003).

The crystallographic information is presented in pole figures in the structural (XYZ) reference frame using equal area projection, upper hemisphere for planes. Equal area is also used for plotting directions but for brevity we only show the relevant pole figures and not both upper and lower hemispheres as conventional for the triclinic crystallography. Data are presented as one point per grain if not otherwise stated. Misorientation axes, i.e. rotation axes, are displayed on pole figures in the structural reference frame (sample coordinate system) using equal area projection, upper hemisphere. Each point in the pole figures for misorientation axes is a misorientation angle calculated between a porphyroclast and an adjacent individual recrystallised grain, between an assumed parent-daughter pair, or between recrystallised grains. Misorientation angle distributions (MAD) showing neighbour pair and random pair misorientation angles are presented in histograms as one point per boundary. Data for shape preferred orientation (SPO; long grain axis vs. short grain axis) were extracted from the EBSD maps. Grain internal strain was estimated following Piazolo et al. (2006) where a grain with average internal misorientation (along a profile) of <1° is denoted substructure-free or "strain-free".

3.3.2. Misorientation data analysis

Deformation mechanisms result in specific crystallographic relationships between the affected grains (Wheeler et al., 2001; Bestmann and Prior, 2003). These grains can be a host grain and daughter grains or an assemblage of recrystallised grains (Jiang et al., 2000; Halfpenny et al., 2006; Warren and Hirth, 2006). Three types of misorientation data have been analysed: 1) misorientation axes across subgrain boundaries have been measured to assess the type of subgrain boundary (e.g. twist or tilt) and possible active slip system-/s (e.g. Lloyd et al., 1997; Kruse et al., 2001; Prior et al., 2002; Piazolo et al., 2008); 2) misorientation axis distributions between porphyroclasts and their neighbour recrystallised grains and between recrystallised grains have been measured to evaluate their crystallographic relationship (e.g. Kruse et al., 2001); 3) MADs from recrystallised assemblages have been measured to assess the deformation mechanisms (e.g. Trimby et al., 1998; Jiang et al., 2000).

4. Results

4.1. Thin section description

In both thin sections (hso468022D and hso468022L) Pl and green Hbl are the two main mineral constituents. Quartz is abundant in the intensely sheared parts as both ribbons and lone grains in the matrix. K-feldspars are present as interstitial grains among recrystallised Pl and as thin films, <30 μm wide, around Qtz grains. Biotite, Ep, Ms, Cal and Chl occur to a minor extent and are localized in or close to thin continuous areas subparallel to mylonitic foliation. These areas of hydrated minerals are interpreted to be late fluid channels and fractures. Opaques and Zrn are accessory phases. Plagioclase grains close to and inside inferred fluid channels exhibit seritisation. Hornblende does not occur as continuous bands in the high strain zone. A phase mixture of recrystallised Hbl and Pl occurs in the tails of Hbl porphyroclasts at the boundary to continuous bands of recrystallised Pl.

Both thin sections (Fig. 2b–f) can be broadly divided into three areas defined by 1) volumetric dominance of a network of Pl porphyroclasts with minor clusters and lenses of recrystallised grains (Fig. 2c–d), 2) areas dominated by mylonitic foliation-defining continuous bands of recrystallised Pl grains and Qtz ribbons along with scattered Pl porphyroclasts (Fig. 2e–f), 3) areas with intense alteration, spatially associated with some of the Qtz ribbons (not shown). Modal mineral content in area (1) and (2) is Pl 75–90%, Hbl 5–20% and Qtz + Kfsp <5%. Quartz content may exceed 50% where Qtz ribbons are abundant. EBSD maps were collected from areas (1) and (2) avoiding alteration zones.

4.1.1. Plagioclase microstructures

Three generations of Pl grains are present in our hand sample (Fig. 2b).

1) Centimetre sized magmatic grains, which are not present in the two thin sections used for EBSD data collection.
2) First generation recrystallised grains with a grain size of >500 μm. These recrystallised grains are referred to as porphyroclasts in this study.

(XYZ). **c–d)** Photomicrographs of plagioclase porphyroclasts and clusters (C1 and C2) and lens L1-2 (EBSD maps L1 and L2) of recrystallised grains. Black boxes are locations of detailed EBSD maps. Black arrows point at grain boundaries with a high angle to mylonitic foliation between plagioclase porphyroclasts where little or no recrystallisation has occurred (see text and Fig. 2g for details). **e–f)** Plagioclase porphyroclasts and continuous bands (B1 and B2) of recrystallised plagioclase. Black boxes show locations of detailed EBSD maps. **g)** Characteristic microstructures in plagioclase porphyroclasts. Note that less recrystallisation occurred along grain boundaries at a high angle to foliation (e.g. grain boundary pointed at by arrow x). Other arrows indicate subgrain walls/boundaries used for slip system interpretations (cf. Fig. 8). **h)** Close-up of recrystallised grains in continuous band B1. Note near polygonal shapes of recrystallised grains and serrated/wavy grain boundaries between porphyroclasts and recrystallised grains. In all thin section micrographs the mylonitic foliation (S) is depicted.

3) Second generation recrystallised grains with an average grain size of 80 μm. From here on "recrystallised grains" refers to this second generation.

Plagioclase porphyroclasts (>500 μm and up to ~4 mm) are dominated by intracrystalline deformation expressed as bent and tapering twins, undulose extinction and development of subgrain boundary walls (Fig. 2g). All porphyroclasts contain subgrain boundaries. The bent albite growth twins continue across subgrain boundary walls and also in some places can be traced across high angle grain boundaries (Fig. 2g). Porphyroclasts are rarely elongated and no general shape preferred orientation is optically recognisable. Some grain boundaries with recrystallised grains have a serrated to wavy appearance (Fig. 2h). Grain boundaries between some of the porphyroclasts display bulges (Fig. 2g). Grain boundaries with a high angle (orientation) to mylonitic foliation show less recrystallisation than grain boundaries subparallel to mylonitic foliation (Fig. 2g).

Recrystallised Pl has a mean grain size of 80 μm with only a few grains present in the size range 150–250 μm. The occurrence of recrystallised grains can be divided into three categories according to the aspect ratio of the encompassing area of the recrystallised grains.

1) *Clusters:* aspect ratio <1:1.5 (Fig. 2c,d); EBSD maps C1 (N = 62) and C2 (N = 25).
2) *Lenses:* aspect ratio > 1:3; subparallel XY (Fig. 2c.); EBSD maps L1 (N = 21) and L2 (N = 68).
3) *Continuous bands* (300–800 μm thick) aspect ratio >1:30; anastamosing; subparallel XY (Fig. 2e–f and h); EBSD maps B1 (N = 60); B1_extended (N = 226; not shown) and B2 (N = 53).

In general, in all three categories, there is a mixture of recrystallised grains with low internal crystal lattice distortion (i.e. strain free) and grains that display strain. Strained grains are evidenced by undulose extinction, deformation twins and rare subgrain boundaries (<2% of the recrystallised grains). Several of the subgrain boundaries are oriented subparallel to mylonitic foliation. Internal distortions such as tapered twins and subgrain boundaries are more common (optically deduced) in clusters and lenses than in the continuous bands. Near equant grains with no internal distortion are more frequent in continuous bands than in clusters or lenses. Grain boundaries are straight or smoothly curved exhibiting 120° triple junctions (Fig. 2h). The average aspect ratio of recrystallised grains in clusters and lenses is 1.88 and in continuous bands 1.79. Recrystallised grains in continuous bands show a weak shape preferred orientation (SPO) with the longest axis at ~45° to the shear zone boundaries (Fig. 3c). No SPO is visible in clusters or lenses of recrystallised grains.

4.1.2. Quartz microstructures

Quartz dominantly occurs as >300 μm wide ribbons oriented parallel to subparallel to the mylonitic foliation. These ribbons are continuous bands consisting of multiple grains and display varied intracrystalline deformation structures (see below). Quartz ribbons in the vicinity of the continuous bands of recrystallised Pl (Fig. 2e) exhibit large amoeboid grains (>700 μm) with lobate grain boundaries, undulatory extinction and many subgrain boundaries. These ribbons cut through Pl porphyroclasts and continuous bands of recrystallised Pl, and contain Pl grains with smooth boundaries. Quartz ribbons in areas with higher amounts of hydrous minerals display a gradual change from large grains with amoeboid grain boundaries to smaller grains with serrated grain boundaries that progressively align with mylonitic foliation.

4.2. Plagioclase composition

Magmatic Pl grains from the less deformed part of the anorthosite-leucogabbro (*M* in Fig. 2b) have an average anorthite content of An79 decreasing to An62 at the rim. The first generation of recrystallised grains (>500 μm) has a composition An42 to An74. The "porphyroclasts" in this study have an average composition of An44 (Fig. 4). The second generation of recrystallised Pl grains which are the focus of this study show an average composition of An 46 (Fig. 4).

4.3. Crystallographic characteristics of plagioclase

4.3.1. Bulk crystallographic preferred orientation (CPO)

The bulk CPO of porphyroclasts (>500 μm) from all EBSD maps is random (Fig. 5a). The bulk CPO of recrystallised grains from all clusters and lenses is also random (Fig. 5b). The bulk CPO from continuous bands of recrystallised grains shows a non-random pattern with the (001) plane aligned with mylonitic foliation and the <010> and <110> with lineation (Fig. 5c).

4.3.2. Grain orientations in recrystallised clusters and lenses

The bulk CPO of recrystallised clusters and lenses shows some clustering (Fig. 5b). Plotting the positions of porphyroclasts adjacent to each of the clusters and lenses in the same pole figures as their neighbouring recrystallised grains shows that the recrystallised grains closest to the porphyroclasts cluster mostly around the orientation of the adjacent porphyroclast (Fig. 6). However, some recrystallised grains appear to have rotated away from the porphyroclast orientation as seen in the pole figures of e.g. directions <001> (Fig. 6d, black arrows).

This close relationship is verified by all but one porphyroclast from the detailed EBSD maps over clusters and lenses marked in Fig. 2. The inconsistency from the one porphyroclast may be a 3D effect.
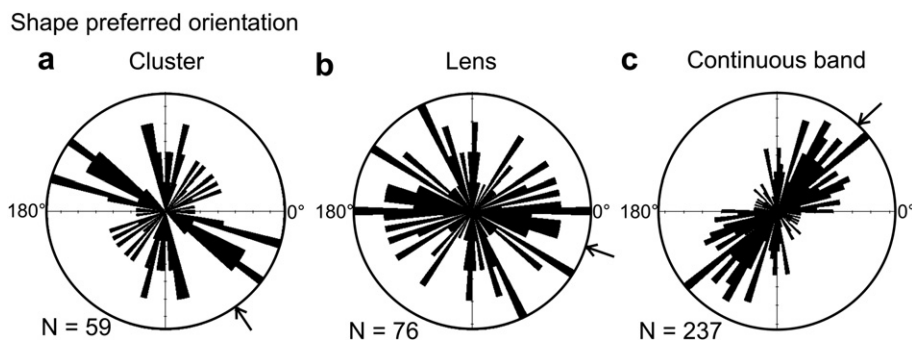

Fig. 3. Orientation of long grain axes with respect to mylonitic foliation (horizontal) of recrystallised plagioclase in **a)** a cluster, **b)** a lens and **c)** a continuous band. Note the shape preferred orientation in the continuous band. Arrows are average densities.
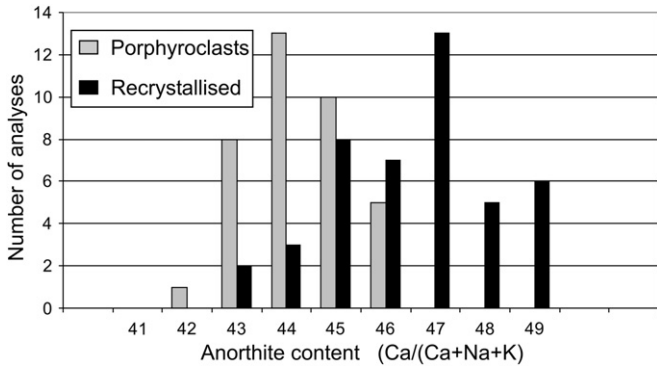
Fig. 4. Plot showing anorthite content in plagioclase porphyroclasts and recrystallised grains.

4.3.3. Grain orientations in recrystallised continuous bands

The bulk CPO in continuous bands shows (001) parallel to mylonitic foliation and <010> and <110> parallel to lineation (Fig. 5c). The orientation of recrystallised grains in physical contact with a porphyroclast (e.g. porphyroclast IV in Fig. 7a) do not plot close to the adjacent porphyroclast orientation, but rather tend to develop the bulk CPO, i.e. rotate to align (001) with XY (Fig. 7b).

4.3.4. Subgrain boundary trace analysis

To assess possible active slip systems we have conducted analyses of misorientation axes across twenty-two subgrain boundaries in recrystallised grains and in porphyroclasts. All analysed boundaries have been verified by a misorientation profile (e.g. Fig. 8a,b). The direction axis that displays the least dispersion in a pole figure, e.g. <201> in Fig. 8c, is assumed the most likely misorientation axis, i.e. the rotation axis (Prior et al., 2002). Each inferred rotation axis has been geometrically compared with possible active slip systems from previously reported TEM studies of plagioclase (Marshall and McLaren, 1977; Olsen and Kohlstedt, 1984; Montardi and Mainprice, 1987; Stünitz et al., 2003). This comparison was conducted in combination with the possible boundary plane orientation taking both tilt and twist boundary geometries into consideration. Furthermore, we assumed that a plausible slip plane should lie subparallel to oblique to the mylonitic foliation (e.g. Fig. 8d).

In general, two slip systems, (010)<001> and (021)<1−12> are consistent with the orientation data obtained. (010)<001> is the
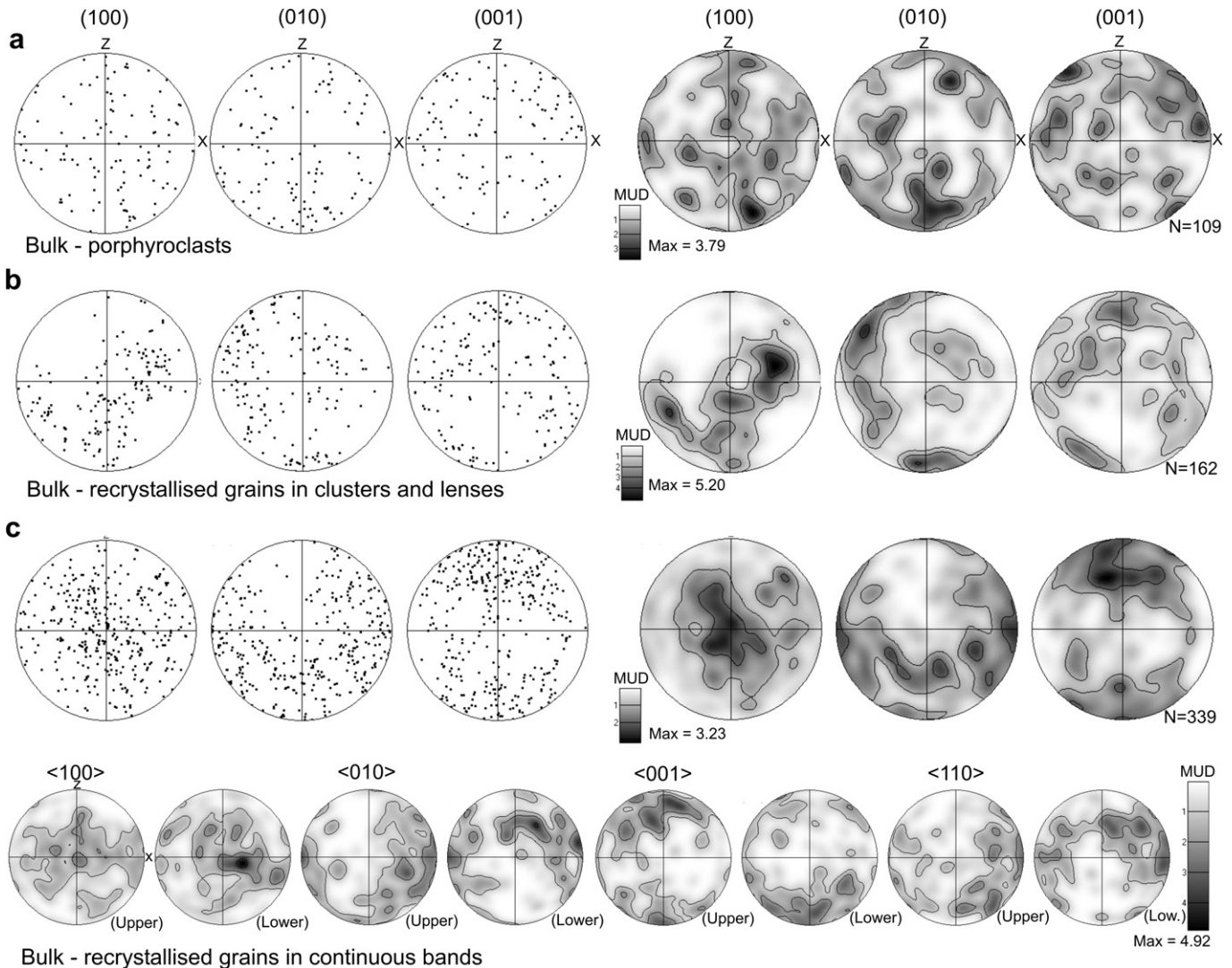

Fig. 5. Pole figures showing the bulk CPO of **a)** plagioclase porphyroclasts from all EBSD maps **b)** two clusters (C1 and C2) and one lens (L1-2) of recrystallised plagioclase grains, **c)** continuous band (B1 and B2). Contours are multiples of a mean uniform distribution (MUD).
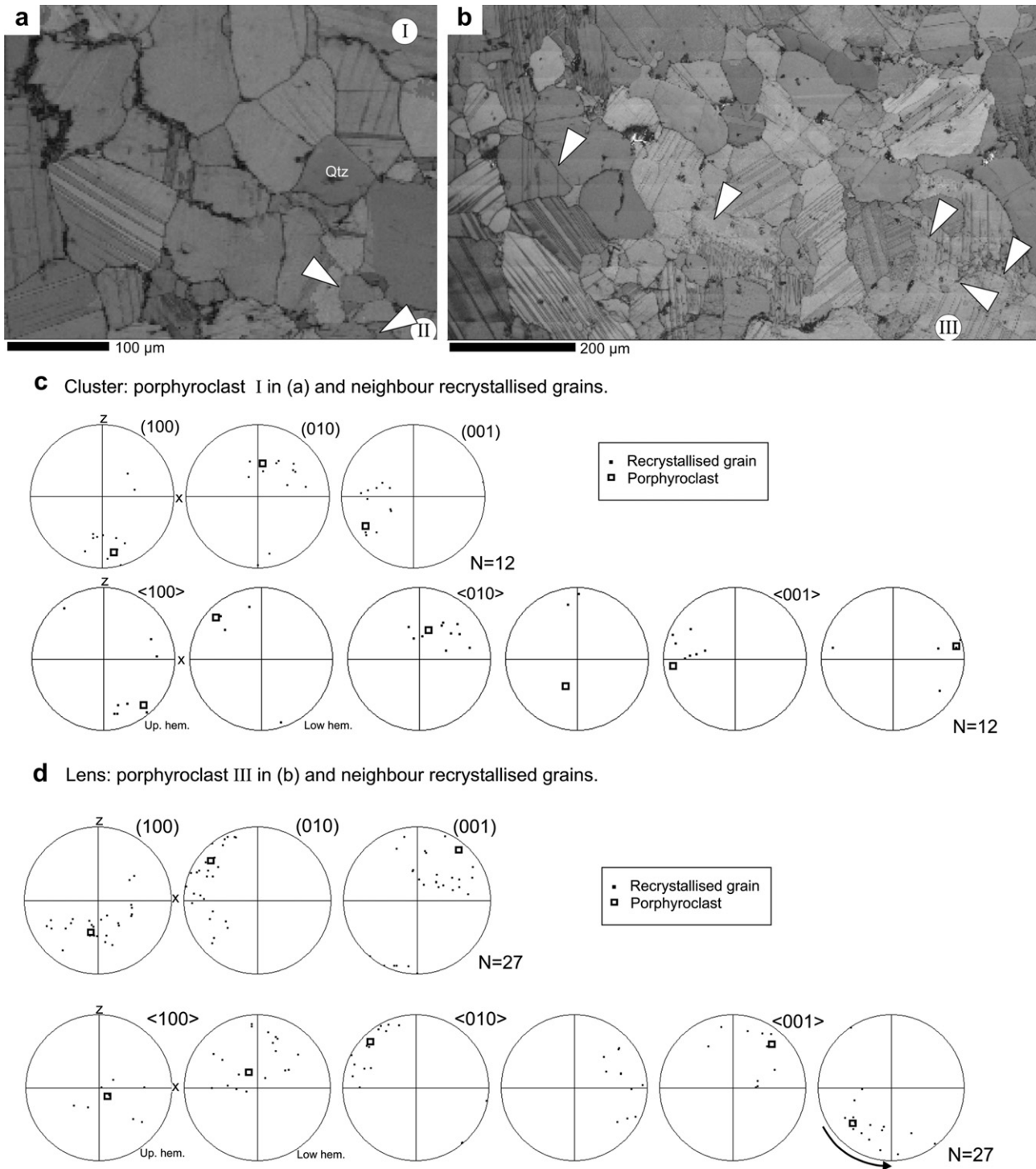
Fig. 6. Band contrast maps (i.e. pattern quality maps) over recrystallised grains in **a)** cluster C2 and **b)** lens L1-2 (Fig. 2d and EBSD map L2 in Fig. 2c, respectively). **c–d)** Pole figures of planes and directions showing crystallographic relationship between porphyroclasts I and III in (a) and (b) and their respective closest recrystallised grains. Note likely rotation of recrystallised grains as indicated by an arrow in (d). Arrows in (a) and (b) refer to subgrain boundaries used in slip system interpretations (cf. Fig. 8).

most commonly found system and is found in combination with at least two but possibly three different rotation axes (Fig. 8d,e). The <101> rotation axis is not perfectly positioned for (010)<001> but gives the best fit of the compared slip systems (Fig. 8e). The two plausible active slip systems are found in both porphyroclasts and recrystallised grains and all analyses are consistent with tilt boundaries cf. Kruse et al., (2001) for explanations about tilt and

twist boundaries in triclinic Pl; Fig. 8d,e). Both slip systems are also represented at the same time within two single porphyroclasts (III in Figs. 2g and 6b, and V in Fig. 7a). However, the orientation of an inferred slip plane is not always found to be oriented suitably with respect to the stress axes (i.e. subparallel to mylonitic foliation). Such an unsuitable orientation is more frequently observed in recrystallised grains than in porphyroclasts.
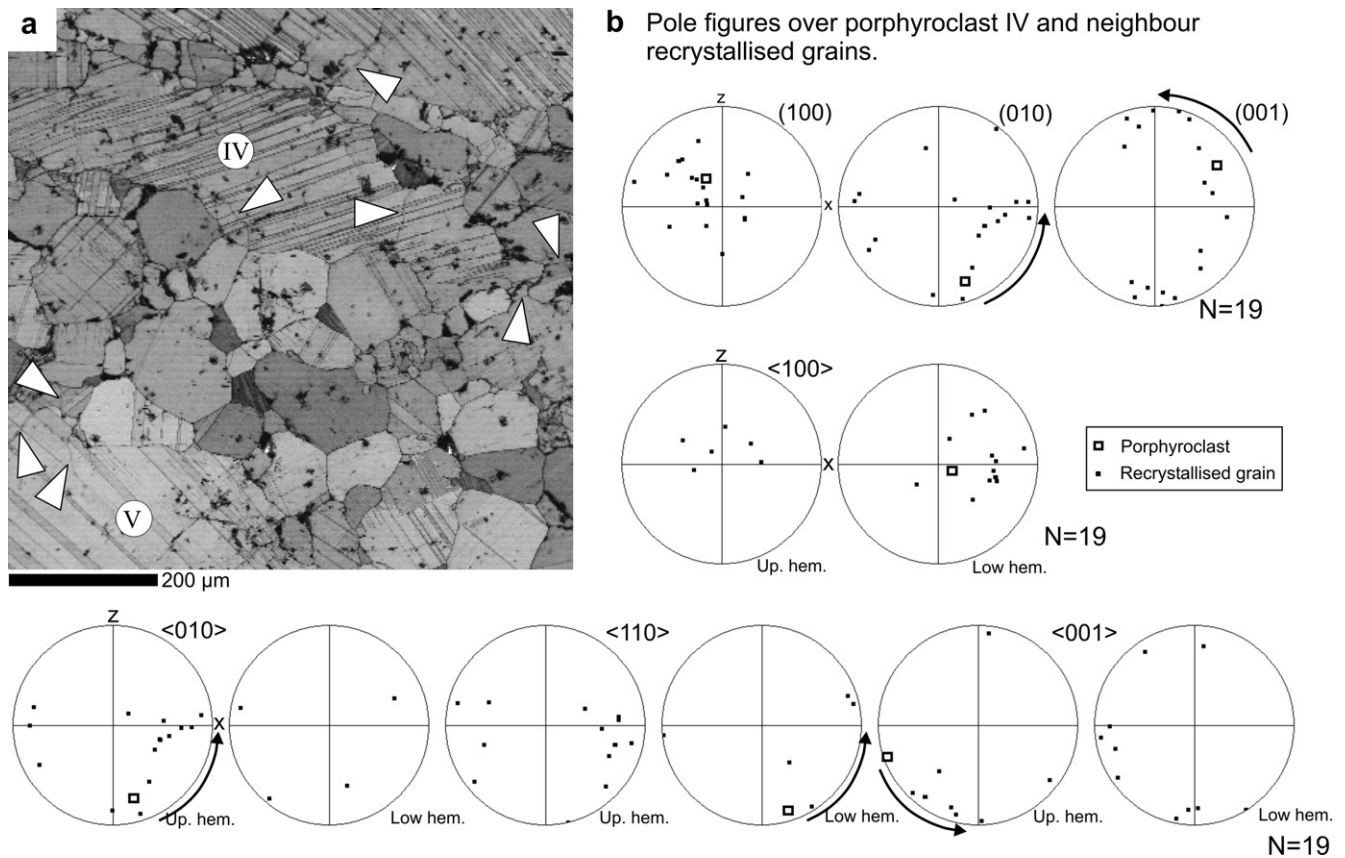
Fig. 7. Crystallographic orientations of recrystallised plagioclase grains in continuous bands and neighbouring porphyroclasts. **a)** Band contrast map over continuous band B1 (cf. Fig. 2e) of recrystallised grains. Arrows refer to subgrain boundaries used in the slip system interpretation (cf. Fig. 8). **b)** Pole figures of planes and directions showing the crystallographic relationship between porphyroclast IV in (a) and neighbour recrystallised grains. Note the rotation of recrystallised grains away from the host orientation to align the (001) plane with mylonitic foliation.

Some subgrain boundaries oriented suitably to the stress axes within porphyroclasts are found with a less suitable orientation in an adjacent recrystallised grain. This scenario occurs e.g. in porphyroclast III (Figs. 2g and 6b) where the orientation of slip plane (021) changes from being subparallel to mylonitic foliation to ~35° to mylonitic foliation in an adjacent recrystallised grain. Subgrain boundaries with slip on the (021)<1–12> system are not found in porphyroclasts oriented with the (010) plane parallel to mylonitic foliation.

4.3.5. Misorientation axis distribution

Misorientation axis distributions between a porphyroclast and adjacent recrystallised grains for a cluster and a lens plot as clusters while the misorientation axes from a continuous band are spread randomly over the pole figure. Furthermore, misorientation axes between recrystallised grains within the same continuous band also show a random distribution (Fig. 9).

4.3.6. Misorientation angle distribution (MAD)

The misorientation angle distribution of recrystallised grains closest to a porphyroclast displays a peak between 10 and 45° with a predominance of <25° (Fig. 10a).

Misorientation angle distributions over recrystallised grains from each category, i.e. a cluster, a lens and a continuous band, show four recognisable trends. Going from the cluster to the lens to the continuous band, there is 1) a decreasing amount of lower angles (10–45°), 2) an increase in the difference between neighbour pairs and random pairs at lower angles (10–45°), 3) a decrease

in the distributions between 60 and 110°, and 4) an increase of high angle (>140°) boundaries (Fig. 10b–d).

5. Interpretation and discussion

5.1. Deformation conditions

The occurrence of orthopyroxene-bearing leucosome ponded in boudin necks in stretched leucogabbro together with metamorphic garnets in the anorthosite and the mineral assemblage of studied samples points to metamorphic conditions corresponding to the PT calculations of a nearby bt–grt–sil bearing metapelite ($T = 675$–700 °C and $P = 350$–450 MPa; Jaconelli, 2009). From microstructures within studied samples and field relationships (e.g. syndeformational leucosome) we infer that the deformation studied here occurred at these conditions. A high deformation temperature is also suggested from the presence of interstitial Kfs and Qtz veins that are interpreted to represent a fluid/melt fraction from the emplacement of the neighbouring Opx-bearing tonalite at a late stage during D2. Furthermore, studied Qtz veins exhibit large amoeboid grains (>700 μm, Fig. 2e) with lobate grain boundaries indicate that high temperature grain boundary migration (GBM) was active (e.g. Passchier and Trouw, 2005). In summary, observations suggest deformation at a lower to mid crustal position ($T = 675$–700 °C and $P = 350$–450 MPa) within a transpressional regime and relatively low bulk strain rates. The latter features are deduced from regional observations such as large-scale folding and
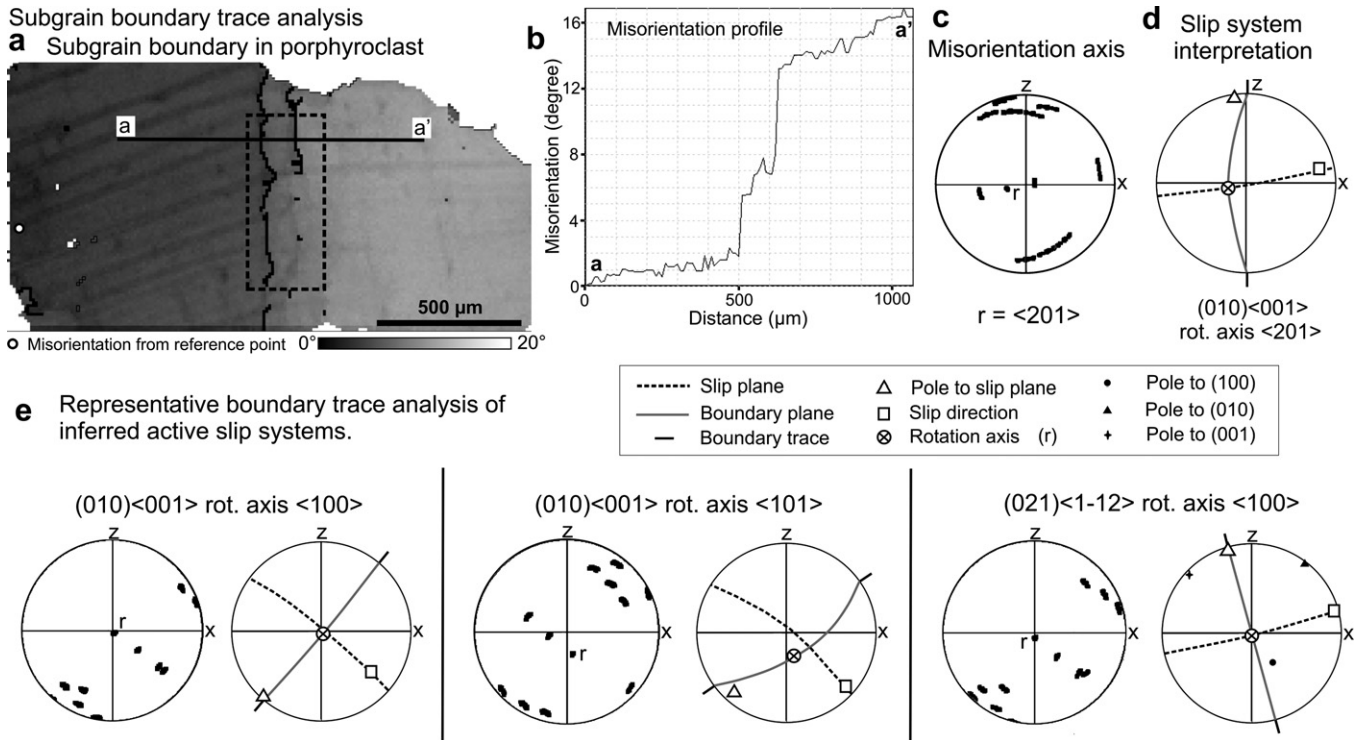
Fig. 8. Representative slip system interpretations from subgrain boundary trace analyses. **a)** Subgrain wall in plagioclase porphyroclast. Misorientation profile a-á is shown in **b)** and data for (c−d) were collected from the stippled box. **c)** Pole figure over crystallographic directions where the axis with the least dispersion (r) is the assumed rotation axis. **d)** Best fit of plausible active slip system with respect to the rotation axis and subgrain boundary trace in (a−c). **e)** Representative boundary trace analyses of assumed active slip systems in plagioclase. Poles to the a-b-c planes are inserted in the last pole figure to show the orientation of the grain.

the width of the tectonised anorthosite-leucogabbro (∼300 m across fold limb).

5.2. Slip systems in plagioclase

Active slip systems in both porphyroclasts and in recrystallised grains were inferred from CPO data and subgrain boundary analyses. Porphyroclasts and recrystallised clusters and lenses do not exhibit a CPO whereas recrystallised grains in continuous bands do (Fig. 5).

In porphyroclasts subgrain boundary analyses indicate that at least two slip systems were active, (010)<001> and (021)<1−12> (Fig. 8). We suggest that (010)<001> is dominant as (a) other workers have shown in natural and experimental samples that

(010)<001> is commonly a dominant slip system (e.g. Olsen and Kohlstedt, 1984; Montardi and Mainprice, 1987; Ji and Mainpraice, 1988; Kruse et al., 2001; Stünitz et al., 2003) and (b) the (021)<1−12> system is only found in a few subgrain boundaries. The latter are seen in porphyroclasts with a hard orientation for (010)<001> slip. Since the (021) plane has a 45° angle to the (010) albite plane, and Kruse et al. (2001) showed that porphyroclasts with a hard orientation responded by fracturing, the (021)< 1−12> system may represent healed microfractures.

The random CPO in recrystallised clusters and lenses is attributed to inheritance of crystallographic orientations from porphyroclasts, as (a) recrystallised grains cluster around the orientations of neighbouring porphyroclasts (Figs. 6 and 9), and (b) subgrain boundaries with the same slip systems characteristics as in the
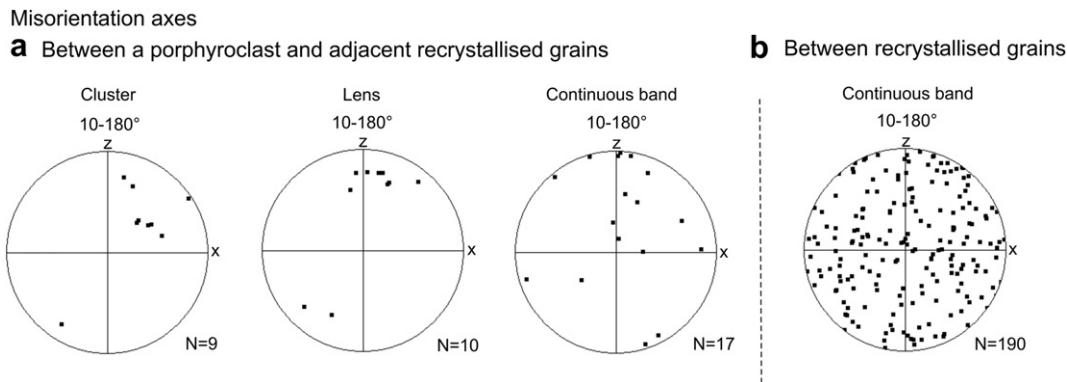

Fig. 9. Distribution of misorientation axes **a)** between a porphyroclast and neighbour recrystallised grains from a cluster (C2; cf. Figs. 2d and 6a), a lens (L2; cf. Figs. 2c and 6b) and a continuous band (B1; cf. Figs. 2e and 7a). Recrystallised grains in the data sets are the ones with physical contact to the selected porphyroclast (one point per grain). **b)** Randomly distributed misorientation axes between recrystallised grains in continuous band B1.
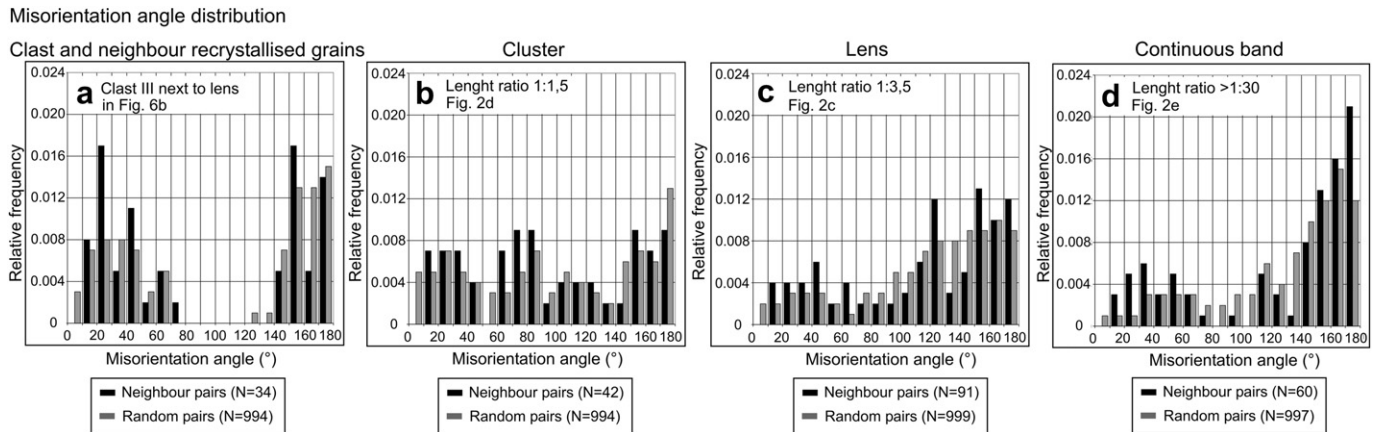
Misorientation angle distribution

Fig. 10. Histograms showing misorientation angle distribution (MAD) between **a)** a plagioclase porphyroclast and neighbouring recrystallised grains in a lens (cf. Fig. 6b) and **b–d)** between recrystallised grains from each category of recrystallised assemblages, as in Fig. 9. Grain boundary angle is set to 10°, i.e. no low angle boundaries are represented in the histograms.

porphyroclasts are present. We suggest that these subgrain boundaries have been inherited from their parent porphyroclast as (i) some subgrain boundaries are unsuitably oriented for slip and (ii) recrystallised grains with subgrain boundaries show twin planes still traceable back to the inferred parent clast (e.g. Fig. 6b).

Recrystallised grains in continuous bands display a CPO where recrystallised grains have rotated to align (001) with the mylonitic foliation and <110> and <010> with the lineation (Figs. 5c and 7b). (001)<110> is the likely dominant slip system in continuous bands of dynamically recrystallised grains since the <010> Burgers vector should not be stable in the C-1 structure (Marshall and McLaren, 1977). Slip on (001) as the dominant plane has been inferred from CPO measurements in naturally and experimentally deformed Pl (e.g. Siegesmund et al., 1994; Heidelbach et al., 2000; Terry and Heidelbach, 2006; Harigane et al., 2008; Kanagawa et al., 2008).

The activation of different slip systems in porphyroclasts and clusters and lenses ((010)<001> and (021)<1–12>), versus that observed in recrystallised bands ((001)<110>) needs to be discussed. Since microstructures represent a continuous development and chemical compositions of all recrystallised grains are similar, temperature cannot be the only governing parameter for the slip system difference. Mehl and Hirth (2008) reported a similar situation in deformed gabbros where porphyroclast deformation occurred on a different slip system than those in adjacent recrystallised layers. They concluded that either the subgrain boundaries in the porphyroclasts are not dominantly composed of the easiest slip system or that the developed CPOs depended on more than just the critical resolved shear stress of the dominant slip system. We suggest that the continuity of the bands gave the recrystallised grains an opportunity to achieve higher strain where a grain size sensitive flow with GBS was activated (see discussion below), allowing the easiest slip system, (001)<110>, to align with mylonitic foliation and lineation (Figs. 5c and 7b). Our observations suggest that grains remaining as porphyroclasts are dominantly oriented unfavourably for slip on (001). Consequently, at 675–700 °C and higher strain (010)<001> and (021)<1–12> are subsidiary slip systems to (001)<110>.

5.3. Deformation mechanisms in plagioclase

5.3.1. Deformation of porphyroclasts and their grain size reduction

Porphyroclasts deformed dominantly by dislocation creep since they exhibit undulose extinction, bending of growth twins and development of subgrain boundaries (e.g. Fig. 2g). Dynamic

recrystallisation of porphyroclasts is interpreted to have taken place by subgrain rotation (SGR; Poirier and Nicolas, 1975; Urai et al., 1986) according to the following: a) subgrains are seen within porphyroclasts, b) subgrains are of similar sizes as recrystallised grains, c) growth twins in porphyroclasts are still traceable into the adjacent recrystallised grains, d) recrystallised grains in clusters/lenses have still orientations close to the adjacent porphyroclast orientation (Fig. 6c–d), d) inheritance of subgrain boundaries from porphyroclast (see above), e) small chemical change from porphyroclast to recrystallised grains showing that recrystallisation is dominantly driven by internal strain energy and not by chemical disequilibrium, and f) high frequency of boundary angles between 10° and 25° as well as some high and very high angle boundaries (>10°, >45°; Fig. 10a). The observed misorientation distribution is consistent with subgrain rotation recrystallisation (Urai et al., 1986; Trimby et al., 1998). Recent studies suggesting that some high and very high angle boundaries are to be expected (Stipp and Kunze, 2008; Mariani et al., 2009) further support our interpretation. Accordingly, the few larger grains (150–250 μm) within the recrystallised matrix are interpreted to represent relict porphyroclasts which are nearly completely recrystallised. However, bulging recrystallisation (e.g. Urai et al., 1986; Hirth and Tullis, 1992) may have been active to a lesser extent as there are some wavy/serrated porphyroclast grain boundaries.

5.3.2. Processes active in clusters, lenses and continuous recrystallised bands

As outlined already in the discussion of slip systems above, clusters and lenses are produced by subgrain rotation but little further inter- and intracrystalline deformation. The straight and smoothly curved grain boundaries and 120° triple junctions observed in all recrystallised categories are consistent with grain boundary adjustment to low energy triple junctions during high temperature deformation (Gottstein and Shvindlerman, 2002; Piazolo et al., 2002).

However, in recrystallised continuous bands additional processes must have been active as here we see the development of a moderately strong CPO, a weak SPO but random misorientation axes between grains (Figs. 3, 5 and 9). The CPO in the continuous bands could be attributed to dislocation creep but we argue here that an additional process was grain boundary sliding accommodated by dislocation glide (DisGBS). DisGBS is a transitional grain size sensitive regime between dislocation creep and diffusion creep

and has been suggested for e.g. calcite (e.g. Rutter et al., 1994), olivine (e.g. Warren and Hirth, 2006 and references therein) and plagioclase (Gómez Barreiro et al., 2007). It involves both glide of dislocations and GBS resulting in the development of a moderate CPO and slight SPO. Rheologically, DisGBS results in Newtonian flow (Gómez Barreiro et al., 2007) where the strain rate limiting factor is balanced between GBS and dislocation glide on the easiest slip system (Warren and Hirth, 2006).

To recognise the DisGBS process in microstructures one must hence find indicators for GBS, grain size sensitivity and dislocation glide. Evidence for GBS has been suggested to include: Randomisation of misorientation axes and weakening of an existing CPO (Jiang et al., 2000; Bestmann and Prior, 2003), low internal strain and equant grain shapes (Passchier and Trouw, 2005), an increase of higher grain boundary angles going from low to high strain areas (Jiang et al., 2000) and phase mixing due to e.g. mechanical mixing or heterogeneous nucleation (e.g. Kruse and Stünitz, 1999; Warren and Hirth, 2006; Dimanov et al., 2007). As a signature for DisGBS,

Prior and Hirth (2007) suggested that misorientation axes between recrystallised grains would be controlled by the deformation kinematics and unrelated to crystallography. Furthermore, the development of a weak to moderate CPO should occur on the easiest slip system (Warren and Hirth, 2006), and this system should be different from the slip systems deduced across subgrain boundaries within adjacent porphyroclasts (Prior and Hirth, 2007). As DisGBS is a grain size sensitive process the preservation of large porphyroclasts is expected if DisGBS is active (Warren and Hirth, 2006). However, to sustain a grain size sensitive mechanism, grain growth must be very slow (i.e. low grain boundary mobility) and/or inhibited by phase mixing (De Bresser et al., 2001).

We suggest that in continuous bands DisGBS is the dominant deformation process. This interpretation is based on: (a) recrystallised grains in continuous bands contains fewer substructures than those in clusters and lenses; (b) several indicators for GBS activity: (b1) progressive rotation of recrystallised grains away from the orientation of the inferred parent porphyroclast (Fig. 7b);
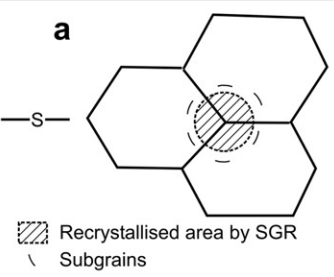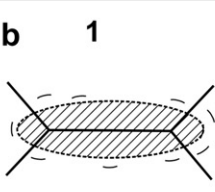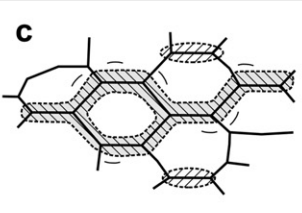
Summary	Cluster	Lens		Continuous band
Stage	**a**	**b** **1**	**2**	**c** ▨ Recrystallised area by SGR + deformed by DisGBS
	▨ Recrystallised area by SGR ＼ Subgrains			
Bulk CPO Porphyroclasts Recrystallised	Random Random	Random Random		Random Non-random, (001)//XY, <110>//X
Grain aspect ratio	1.88	1.88		1.79
SPO	no	no		yes
Slip systems Porphyroclasts Recrystallised	(010)<001>, (021)<1-12> Same as parent clast	As in (a) As in (a)		As in (a) From CPO - single dominant slip system, (001)<110>
Misorientation axes	Clustering	Clustering		Random
Misorientation angle distr.	Dominantly lower angles (< 45°).	Lower angles (< 45°) are more prominent than higher angles (> 140°).		Increase of higher angle grain boundaries compared to cluster and lenses.
Processes	Stress concentration at triple points of porphyroclasts. Dislocation creep. Subgrain rotation recrystallisation.	b.1) Same as for (a) + propagation of recrystallised area subparallel to the XY plane. b.2) Less recrystallisation along boundaries subperpendicular to foliation.		Development of continuous bands by coalescence of clusters and lenses. Local phase mixing. Inferred activation of disGBS, strain localisation and rheological weakening.

Fig. 11. Conceptual model for onset of strain localisation in plagioclase-rich rocks. **a)** Initiation of dynamic recrystallisation by SGR at triple junctions between porphyroclasts produces clusters of recrystallised grains. **b1)** Lenses are developed by coalescence of clusters as the recrystallisation process propagates along grain boundaries oriented subparallel to shear zone boundaries. **b2)** Recrystallisation occurs less frequently along grain boundaries at a high angle to mylonitic foliation (e.g. Fig. 2g). **c)** Continuous bands of recrystallised grains develop subparallel (anastamosing) to shear zone boundaries as continued recrystallisation causes coalescence of clusters and lenses. These continuous bands allow strain localisation due to breaking of the porphyroclast network, grain size reduction, CPO development and possible shift in deformation mechanism. Once coalesced very little further strain or dynamic recrystallisation of porphyroclasts occurs.

(b2) increase of higher grain boundary angles going from cluster to lens to continuous band (Fig. 10b–d); (b3) development of an SPO while retaining grain aspect ratios similar to those in clusters and lenses (Fig. 3); (b4) local phase mixing of Hbl and Pl in the tails of Hbl porphyroclasts and presence of interstitial Kfs (inferred melt/fluid fraction filling voids) as films along some of the grain boundaries and in triple junctions; (b5) random misorientation axes (Fig. 9); (c) slip systems within porphyroclasts are different than the slip system from CPO of continuous bands; (d) large and variable grain size of porphyroclasts; (e) the recrystallised grain size (average 80 μm) is close to the experimentally deduced boundary between the fields of dislocation creep and diffusion creep (Rybacki and Dresen, 2004).

The only previously suggested indicator for DisGBS not seen in our samples is the systematic reorientation of misorientation axes with respect to the kinematic coordinate system (Prior and Hirth, 2007). This may be due to too large rigid body grain rotations to sustain a consistency of misorientation axes and/or the misorientation pattern may have been disturbed by grain boundary pinning by the inferred fluid/melt fraction, from where Qtz veins and the interstitial Kfs crystallised.

The observed low internal strain and presence of few subgrain boundaries in recrystallised grains could be attributed to post-deformational annealing (Heilbronner and Tullis, 2002). However, porphyroclasts still show an abundance of subgrains and the sizes of the observed subgrains within porphyroclasts are similar to the size of recrystallised grains indicating that annealing did not occur to the extent that it changed the microstructure significantly.

5.4. Onset of dynamic recrystallisation and strain localisation

On the basis of the above discussion, we suggest a conceptual model for the development of recrystallisation and initial strain localisation within developing continuous bands of recrystallised grains at temperatures of 675–700 °C and moderate pressure (Fig. 11).

In the initial stage (Stage 1) stress is concentrated at large grain triple junctions. The stress-induced higher dislocation density close to the boundaries of these grains results in subgrain formation and subsequent grain size reduction by SGR. Clusters of recrystallised grains are produced (Fig. 2c,d, 11a). Further deformation (Stage 2) results in stress concentration at clast-recrystallised grain boundaries and causes propagation of SGR recrystallisation along grain boundaries suitably aligned with respect to the stress field i.e. subparallel to the simple shear component (Fig. 11b.1). This localisation of recrystallisation causes clusters to coalesce and form lenses of recrystallised grains aligned subparallel with mylonitic foliation (Fig. 2c) similar to numerical results shown by Piazolo et al. (2002). Then (Stage 3) clusters and lenses continued to coalescence parallel-/subparallel to the shear plane developing an anastamosing network of continuous bands (Fig. 2e–f, 2h and 11c). Now, DisGBS can become a significant process as GBS is geometrically possible (Halfpenny et al., 2006). These bands are rheologically weaker than the framework of porphyroclasts due to grain size reduction, the development of a geometrical softening i.e. a CPO (Tullis and Yund, 1985; Urai et al., 1986; Ji and Mainpraice, 1990) and change in deformation mechanism from dislocation creep to DisGBS with Neutonian flow behaviour (Dimanov et al., 2007; Gómez Barreiro et al., 2007). These bands thus represent a connectivity of weak zones and as such, once formed, will accommodate most if not all strain and therefore no further (or only minor) deformation of porphyroclasts occurs. Hence, the porphyroclasts are preserved and not completely recrystallised.

As a consequence, the rheology of the rock is governed by the recrystallised bands i.e. Newtonian flow. The development of a CPO *could* have been misinterpreted as a result of dislocation creep alone, if misorientation analyses were not performed, and then the strength of the high strain zone would have been overestimated.

6. Conclusions

To investigate the mechanisms for onset of recrystallisation and strain localisation in a deformed anorthosite-leucogabbro detailed microstructural analyses were performed on Pl porphyroclasts and their recrystallised grains which show successive development into clusters, lenses and continuous bands. Deformation is estimated to have occurred at temperatures of ~675–700 °C, at moderate pressure (~350–450 MPa). Our main observations are

- Plagioclase porphyroclasts are deformed by dislocation creep and recrystallised mainly by SGR. Bulk CPO is random but subgrain boundary trace analysis indicate dominance of slip system (010)<001>, while (021)<1–12> is subsidiary.
- Recrystallised grains (average grain size 80 μm) found in clusters at triple junctions of porphyroclasts and in lenses aligned with mylonitic foliation show the same active slip systems and similar crystallographic orientation as their parent porphyroclasts.
- Recrystallised grains in anastamosing continuous bands display a weak to moderate SPO and a moderately developed CPO consistent with the main slip system (001)<110>.

According to these observations, we suggest that with increasing strain and recrystallisation, clusters and lenses coalesce and produce interconnected anastamosing bands of recrystallised grains. Microstructures and crystallographic relationships within the recrystallised bands are consistent with dislocation glide in combination with GBS indicating the activity of the grain size sensitive process DisGBS. The inferred shift in deformation mechanism results in a change of flow law which significantly lowers the strength of the deforming rock. Together with weakening due to CPO development and grain size reduction, strain is localized in these connected networks of weak anastamosing recrystallised bands. Once these bands are formed, deformation is largely localized in those zones and the remainder of the rock does not further deform. As a consequence, the flow law of the partly recrystallised anorthosite-leucogabbro follows a Newtonian flow law.

References

Adams, B.L., Wright, S.I., Kunze, K., 1993. Orientation imaging: the emergence of a new microscopy. Metallurgical Transactions 24A, 819–831.

Baratoux, L., Schulmann, K., Ulrich, S., Lexa, O., 2005. Contrasting microstructures and deformation mechanisms in metagabbro mylonites contemporaneously deformed under different temperatures (c. 650°C and c. 750°C). In: Gapais, D., Brun, J.P., Cobbold, P.R. (Eds.), Deformation Mechanisms, Rheology and Tectonics: from Minerals to the Lithosphere. Geological Society, London. Special Publications, 243, pp. 97–125.

Bestmann, M., Prior, D.J., 2003. Intragranular dynamic recrystallization in naturally deformed calcite marble: diffusion accommodated grain boundary sliding as a result of subgrain rotation recrystallisation. Journal of Structural Geology 25, 1597–1613.

Crowley, J.L., 2002. Testing the model of late Archean terrane accretion in southern West Greenland: a comparison of the timing of geological events across the Qarliit nunaat fault, Buksefjorden region. Precambrian Research 116, 57–79.

De Bresser, J.H.P., Ter Heege, J.H., Spiers, C.J., 2001. Grain size reduction by dynamic recrystallization: can it result in major rheological weakening? International Journal of Earth Sciences (Geol Rundsch) 90, 28–45.

Dimanov, A., Rybacki, E., Wirth, R., Dresen, G., 2007. Creep and strain-dependent microstructures of synthetic Anorthite-diopside aggregates. Journal of Structural Geology 29, 1049–1069.

Fitz Gerald, J.D., Parise, J.B., Mackinnon, I.D.R., 1986. Average structure of an An$_{48}$ plagioclase from the Hogarth Ranges. American Mineralogist 71, 1399–1408.

Friend, C.R.L., Nutman, A.P., 2005. New pieces to the Archaean jigsawpuzzle in the Nuuk region, southern West Greenland: steps in transforming a simple insight into a complex regional tectonothermal model. Journal of the Geological Society (London) 162, 147–162.

Friend, C.R.L., Nutman, A.P., McGregor, V.R., 1987. Late-Archaean tectonics in the Færingehavn – Tre Brødre area, south of Buksefjorden, southern west Greenland. Journal of the Geological Society (London) 144, 369–376.

Gómez Barreiro, J., Lonardelli, I., Wenk, H.R., Dresen, G., Rybacki, E., Ren, Y., Tomé, C.N., 2007. Preferred orientation of anorthite deformed experimentally in Newtonian creep. Earth and Planetary Science Letters 264, 188–207.

Gottstein, G., Shvindlerman, L.S., 2002. Triple junction drag and grain growth in 2D polycrystals. Acta Materialia 50, 703–713.

Halfpenny, A., Prior, D.J., Wheeler, J., 2006. Analysis of dynamic recrystallisation and nucleation in a quartzite mylonite. Tectonophysics 427, 3–14.

Harigane, Y., Michibayashi, K., Ohara, Y., 2008. Shearing within lower crust during progressive retrogression: structural analysis of gabbroic rocks from the Godzilla Mullion, an oceanic core complex in the Parece Vela backarc basin. Tectonophysics 457, 183–196.

Heidelbach, F., Post, A., Tullis, J., 2000. Crystallographic preferred orientation in albite samples deformed experimentally by dislocation and solution precipitation creep. Journal of Structural Geology 22, 1649–1661.

Heilbronner, R., Tullis, J., 2002. The effect of static annealing on microstructures and crystallographic preferred orientations of quartzites experimentally deformed in axial compression. In: de Meer, S., Drury, M.R., de Bresser, J.H.P., Pennock, G.M. (Eds.), Deformation Mechanisms, Rheology and Tectonics: Current Status and Future Perspectives. Geological Society of London,Special Publication, vol. 200, pp. 191–218.

Hirth, G., Tullis, J., 1992. Dislocation creep regimes in quartz aggregates. Journal of Structural Geology 14, 145–159.

Jaconelli, P., 2009. Quantitative Analysis of Sillimanite Microstructures in Naturally Deformed Rocks: An EBSD Study. Ms Thesis. Stockholm University, 69 pp.

Ji, S., Mainpraice, D., 1988. Natural deformation fabrics of plagioclase: implications for slip systems and seismic anisotropy. Tectonophysics 147, 145–163.

Ji, S., Mainpraice, D., 1990. Recryztallisation and fabric development in plagioclase. Journal of Geology 98, 65–79.

Jiang, Z., Prior, D.J., Wheeler, J., 2000. Albite crystallographic preferred orientation and grain misorientation distribution in a low-grade mylonite: implications for granular flow. Journal of Structural Geology 22, 1663–1674.

Kanagawa, K., Shimano, H., Hiroi, Y., 2008. Mylonitic deformation of gabbro in the lower crust: a case study from the Pankenushi gabbro in the Hidaka metamorphic belt of central Hokkaido, Japan. Journal of Structural Geology 30, 1150–1166.

Kenkmann, T., Dresen, G., 2002. Dislocation microstructure and phase distribution in a lower crustal shear zone – an example from the Ivrea-Zone, Italy. International Journal of Earth Sciences (Geol. Rundsch.) 91, 445–458.

Kretz, R., 1983. Symbols for rock-forming minerals. American Mineralogist 68, 277–279.

Kruse, R., Stünitz, H., 1999. Deformation mechanisms and phase distribution in mafic high-temperature mylonites from the Jotun Nappe, southern Norway. Tectonophysics 303, 223–249.

Kruse, R., Stünitz, H., Kunze, K., 2001. Dynamic recrystallization processes in Plagioclase porphyroclasts. Journal of Structural Geology 23, 1781–1802.

Lee, N.R., Hollis, J., Harley, S., Herwartz, D., 2006. Field report – Qarliit Nunaat. The Geological Survey of Denmark and Greenland, unpublished.

Lloyd, G.E., Farmer, A.B., Mainprice, D., 1997. Misorientation analysis and the formation and rotation of subgrain and grain boundaries. Tectonophysics 279, 55–78.

Mariani, E., Mecklenburgh, J., Wheeler, J., Prior, D.J., Heidelbach, F., 2009. Microstructure evolution and recrystallization during creep of MgO single crystals. Acta Materialia 57, 1886–1898.

Marshall, D.B., McLaren, A.C., 1977. The direct observation and analysis of dislocations in experimentally deformed plagioclase feldspars. Journal of Materials Science 12, 893–903.

Mehl, L., Hirth, G., 2008. Plagioclase preferred orientation in layered mylonites: evaluation of flow laws for the lower crust. Journal of Geophysical Research 113 B05202.

Montardi, Y., Mainprice, D.A., 1987. Transmission electron microscopic study of the natural plastic deformation of plagioclase (An68–70). Bulletin of Mineralogy 110, 1–14.

Montési, L.G.J., Hirth, G., 2003. Grain size evolution and the rheology of ductile shear zones: from laboratory experiments to postseismic creep. Earth and Planetary Science Letters 211, 97–110.

Nutman, A.P., Friend, C.R.L., Baadsgaard, H., McGregor, V.R., 1989. Evolution and assembly of Archean gneiss terranes in the Godthåbsfjord region, southern West Greenland: structural, metamorphic and isotopic evidence. Tectonics 8, 573–589.

Olsen, T.S., Kohlstedt, D.L., 1984. Analysis of dislocations in some naturally deformed plagioclase feldspars. Physics and Chemistry of Minerals 11, 153–160.

Owens, B.E., Dymek, R.F., 1997. Comparative petrology of Archaean anorthosites in amphibolite and granulite facies terranes, SW Greenland. Contributions to Mineralogy and Petrology 128, 371–384.

Passchier, C.W., Trouw, R.A.J., 2005. Microtectonics, second ed. Springer-Verlag, Berlin Heidelberg, pp 366.

Piazolo, S., Montagnat, M., Blackford, J.R., 2008. Sub-structure characterization of experimentally and naturally deformed ice using cryo-EBSD. Journal of Microscopy 230, 509–519.

Piazolo, S., Bestmann, M., Prior, D.J., Spiers, C.J., 2006. Temperature dependent grain boundary migration in deformed-then-annealed material: observations from experimentally deformed synthetic rocksalt. Tectonophysics 427, 55–71.

Piazolo, S., Bons, P.D., Jessell, M.W., Evans, L., Passchier, C.W., 2002. Dominance of Microstructural Processes and Their Effect on Microstructural Development: Insights from Numerical Modelling of Dynamic Recrystallization. In: Geological Society of London, Special Publications, 200 149–170.

Poirier, J.P., Nicolas, A., 1975. Deformation induced recrystallisation due to progressive misorientation of subgrains, with special reference to mantle peridotites. Journal of Geology 83, 707–720.

Prior, D.J., Hirth, G., 2007. Microstructural recognition of grain boundary sliding and its rheological implications. Rend. Soc. Geol. It. 5, 187. DRT conference abstract.

Prior, D.J., Wheeler, J., Peruzzo, L., Speiss, R., Storey, C., 2002. Some garnet microstructures: an illustration of the potential of orientation maps and misorientation analysis in microstructural studies. Journal of Structural Geology 24, 999–1011.

Prior, D.J., Boyle, A.P., Brenker, F., Cheadle, M.C., Day, A., Lopez, G., Peruzzo, L., Potts, G.J., Reddy, S., Spiess, R., Timms, N.E., Trimby, P., Wheeler, J., Zetterström, L., 1999. The application of electron backscatter diffraction and orientation contrast imaging in the SEM to textural problems in rocks. American Mineralogist 84, 1741–1759.

Raimbourg, H., Toyoshima, T., Harima, Y., Kimura, G., 2008. Grain-size reduction mechanisms and rheological consequences in high-temperature gabbro mylonites of Hidaka, Japan. Earth and Planetary Science Letters 267, 637–653.

Rutter, E.H., Brodie, K.H., 1988. The role of tectonic grain size reduction in the Rheological stratification of the lithosphere. International Journal of Earth Sciences (Geol. Rundsch.) 77, 295–308.

Rutter, E.H., Casey, M., Burlini, L., 1994. Preferred crystallographic orientation development during the plastic and superplastic flow of calcite rocks. Journal of Structural Geology 16, 1431–1446.

Rybacki, E., Dresen, G., 2004. Deformation mechanism maps for feldspar rocks. Tectonophysics 382, 173–187.

Siegesmund, S., Helming, K., Kruse, R., 1994. Complete texture analysis of a deformed amphibolite: comparison between neutron diffraction and U-stage data. Journal of Structural Geology 16, 131–142.

Stipp, M., Kunze, K., 2008. Dynamic recrystallisation near the brittle-plastic transition in naturally and experimentally deformed quartz aggregates. Tectonophysics 488, 77–97.

Stünitz, H., Fitz Gerald, J.D., Tullis, J., 2003. Dislocation generation, slip-systems, and dynamic recrystallization in experimentally deformed plagioclase single crystals. Tectonophysics 372, 215–233.

Terry, M.P., Heidelbach, F., 2006. Deformation-enhanced metamorphic reactions and the rheology of high-pressure shear zones, Western Gneiss region, Norway. Journal of Metamorphic Geology 24, 3–18.

Trimby, P.W., Prior, D.J., Wheeler, J., 1998. Grain boundary hierarchy development in a quartz mylonite. Journal of Structural Geology 20, 917–935.

Tullis, J., 2002. Deformation of granitic rocks: experimental studies and natural examples. In: Karato, S., Wenk., H.-R. (Eds.), Plastic Deformation of Minerals and Rocks. Reviews in Mineralogy and Geochemistry, 51, pp. 51–95.

Tullis, J., Yund, R., 1985. Dynamic recrystallisation of feldspar mechanism for ductile shear zone formation. Geology 13, 238–241.

Urai, J.L., Means, W.D., Lister, G.S., 1986. Dynamic recrystallisation of minerals. In: Hobbs, B.E., Heard, H.C. (Eds.), Mineral and Rock Deformation (Laboratory Studies). Geophysical Monograph of the American Geophysical Union, 36, pp. 161–200.

Warren, J.C., Hirth, G., 2006. Grain size sensitive deformation mechanisms in naturally deformed peridotites. Earth and Planetary Science Letters 248, 438–450.

Wheeler, J., Prior, D.J., Jiang, Z., Spiess, R., Trimby, P., 2001. The petrological significance of misorientations between grains. Contributions to Mineralogy and Petrology 141, 109–124.

White, S.H., Burrows, S.E., Carreras, J., Shaw, N.D., Humphreys, F.J., 1980. On mylonites in ductile shear zones. Journal of Structural Geology 2, 175–187.